Journal of Power Sources 247 (2014) 981–990

Contents lists available at ScienceDirect

Journal of Power Sources

journal homepage: www.elsevier.com/locate/jpowsour

Analysis of solid electrolyte interface formation reaction and surface deposit of natural graphite negative electrode employing polyacrylic acid as a binder

Koichi Ui [a, *], Daisuke Fujii [a], Yuki Niwata [a], Tomohiro Karouji [a], Yu Shibata [a], Yoshihiro Kadoma [a], Kazuaki Shimada [b], Naoaki Kumagai [a]

[a] Department of Frontier Materials and Function Engineering, Graduate School of Engineering, Iwate University, 4-3-5 Ueda, Morioka, Iwate 020-8551, Japan
[b] Department of Chemistry and Bioengineering, Graduate School of Engineering, Iwate University, 4-3-5 Ueda, Morioka, Iwate 020-8551, Japan

HIGHLIGHTS

- The XPS spectra of C1s region for NG-3 electrode after discharging up to 2.0 V is shown.
- The NG-3 electrodes using PAA and PVdF as the binders, respectively are shown.
- The amount of the inorganic components of the SEI was low in the case of the PAA binder.
- The binder types have an influence on the SEI composition.

GRAPHICAL ABSTRACT

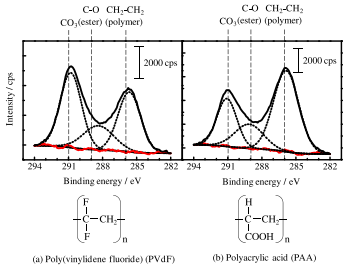

High resolution XPS spectra (—), fitting curves (····), and the error (—)

ARTICLE INFO

Article history:
Received 9 April 2013
Received in revised form
8 August 2013
Accepted 21 August 2013
Available online 3 September 2013

Keywords:
Lithium-ion battery
Natural graphite
Negative electrode
Polyacrylic acid
Binder
Solid electrolyte interface (SEI)

ABSTRACT

We analyzed the solid electrolyte interface (SEI) formation reaction and surface deposit of a natural graphite (NG-3) electrode employing polyacrylic acid (PAA) as a binder in an ethylene carbonate-based electrolyte because it was reported that the initial charge–discharge characteristics of the NG-3 electrode were improved by employing the PAA binder. Poly(vinylidene fluoride) as a binder was used for comparison. We investigated the influence of the binder types on the coating of the NG-3 particles using the B.E.T. specific surface areas. The difference in the above phenomenon was explained by the relationship between the B.E.T. specific surface area and the irreversible capacity. The surface chemical composition of the NG-3 electrode was investigated by FE-SEM/EDX and XPS and then the difference between the PAA binder and the PVdF binder was discussed. The FE-SEM/EDX and the XPS results showed that the amount of the inorganic components of the SEI was relatively small in the case of the PAA binder NG-3 electrode. The AC impedance results showed that the SEI film resistance of the PAA binder NG-3 electrode was lower at 0.2 V. It was clarified that the binder types affected the coating state, the SEI formation reaction, and the SEI film composition.

1. Introduction

Various improvements in the electrochemical characteristics of the graphite electrode have been reported. As an example, the initial irreversible capacity of the graphite electrode in an ethylene carbonate (EC)-based electrolyte was reduced by employing gelatin as a binder [1,2]. In addition, the same research group reported that the initial irreversible capacity of the graphite electrode in the EC-based electrolyte was reduced by employing a water-soluble polymer of sodium carboxymethyl cellulose (CMC-Na) as a binder [3]. In recent years, it has been reported that the contact area

* Corresponding author. Tel.: +81 19 621 6340; fax: +81 19 621 6314.
E-mail address: kui@iwate-u.ac.jp (K. Ui).

0378-7753/$ – see front matter © 2013 Elsevier B.V. All rights reserved.
http://dx.doi.org/10.1016/j.jpowsour.2013.08.083

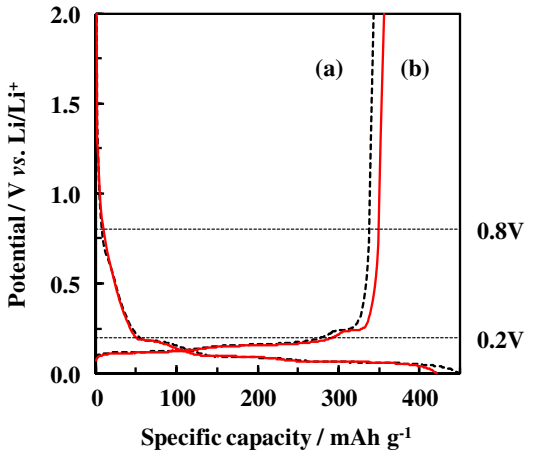

Fig. 1. 1st charge–discharge curves of NG-3 electrodes using (a) PVdF 10 wt. % and (b) PAA 10 wt. % as the binders in the 1 mol dm^{-3} $LiClO_4$/EC + DEC (50:50 vol. %) electrolyte [5]; potential range: 5 mV–2.0 V *vs.* Li/Li^+; current density: 175 mA g^{-1} (0.5 C); (——) PAA 10wt. %; (– – – -) PVdF 10 wt. %.

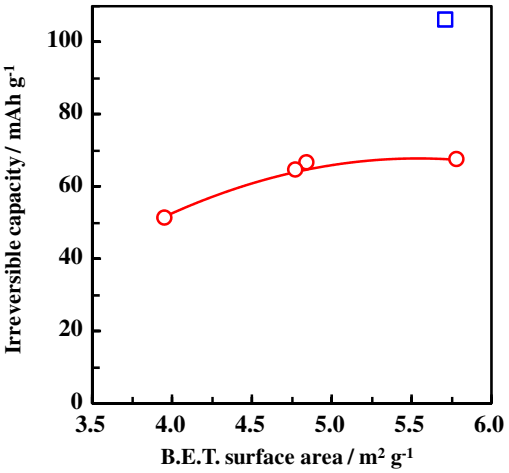

Fig. 3. Relationship between the B.E.T. specific surface area of NG-3 electrodes and the irreversible capacity of 1st cycle; (○) PAA 10 wt. %; (□) PVdF 10 wt. %. Solid curve indicates trend in the experimental data.

between the $LiCoO_2$ particles and graphite particles increased because both the $LiCoO_2$ and graphite powders were effectively dispersed by employing ammonium polyacrylic acid (PAA–NH_4) as a dispersant, resulting in the improved charge–discharge characteristics of the $LiCoO_2$ electrode [4].

Based on these reports, we have focused on a water-soluble polymer of polyacrylic acid (PAA) as the binder and covering agent. Our group has reported that the graphite particle coated with PAA enabled the reversible charge (Li^+ ion intercalation) and discharge (deintercalation) reaction in a propylene carbonate (PC)-based electrolyte; it could effectively improve the charge–discharge characteristics in an EC-based electrolyte [5]. The PAA as a binder for the natural graphite negative electrode [6], for the Si alloy negative electrode [7], and $LiFePO_4$ positive electrode [8] was then reported for use in a lithium-ion battery. However, the detailed mechanism, which PAA exerts on the improvement of the charge–discharge characteristics, has not yet been clarified.

In this study, we focused on the coating state of the graphite particles coated with PAA, the surface deposit of the NG-3 electrode, and the solid electrolyte interface (SEI) formation reaction during the initial charging because it was considered that they would have an influence on the initial charge–discharge characteristics. Considering the further design of a novel binder, we analyzed of the SEI formation reaction and the chemical composition of the surface deposit to obtain primary knowledge about the natural graphite electrode coated with PAA. We have discussed the influence of the difference in the binder types on the SEI formation reaction and the chemical composition of the surface deposit by mainly analyzing the change in the natural graphite electrode surface during the initial charge–discharge cycling.

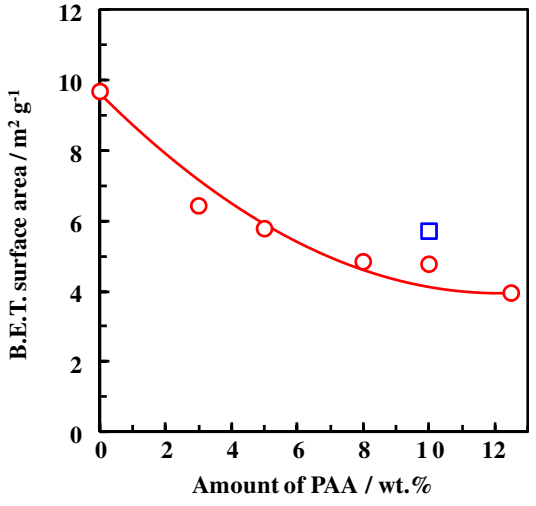

Fig. 2. B.E.T. specific surface area of NG-3 electrodes using the prescribed amount of PVdF and PAA as the binders before charging; (○) PAA 10 wt. %; (□) PVdF 10 wt. %.

2. Experimental

The graphite electrode was prepared in a way similar to that previously reported [9]. Natural graphite powder (Kansai Coke and Chemical Co., NG-3) as the active material, PAA (Wako Pure Chemical Industries, Ltd.; average molecular weight, 1,000,000) as the binder, and poly(vinylidene fluoride) (Kureha. Co., KF polymer #9130, PVdF) for comparison were employed. A suspension composed of 90 wt. % NG-3 powder and 10 wt. % binder was prepared using a dispersing medium and was then stirred in a reagent bottle at room temperature for 24 h. The percentages by mass of the electrode material in the suspension for the PAA-NG-3 suspension (primarily distilled water as the dispersing medium) and the PVdF-NG-3 suspension (*N*-methyl-2-pyrrolidone (Kanto Chemical Co., 99.0%, NMP) as the dispersing medium) were 20.0 wt. % and 43.5 wt. %, respectively. The suspension was coated on a Ni mesh (Tokyo Screen Co., 100 mesh, 10 mm × 10 mm). The electrode was then pressed for 10 min after air-drying at 80 °C for 1 h. Prior to their use, the PAA-NG-3 electrode and the PVdF-NG-3 electrode were dried in a vacuum at 200 °C and 180 °C for 3 h, respectively.

A three-electrode cell, which consisted of the NG-3 electrode (W.E.), a pressed lithium metal foil on the Ni mesh (R.E. and C.E.), and a 1 mol dm^{-3} (M) solution of $LiClO_4$ in EC:DEC (diethyl carbonate) (50:50 vol. %) (Mitsubishi Chemical Co.; water content under 10 ppm) as the electrolyte, was employed for the electrochemical measurements. The cells were assembled in a glove box (Miwa Mtg Co., Ltd., DBO-1NKP-1U-2) filled with dry argon at 25 °C. The charge–discharge cycle tests were performed using an automatic battery charging–discharging instrument (Hokuto Denko, HJR1010mSM8) at the current density of 175 mA g^{-1}(1C = 350 mA g^{-1}) between 5 mV and 2.0 V at 25 °C. The AC impedance apparatus consisted of a computer-controlled electrochemical measuring system (Hokuto Denko HZ-5000) and

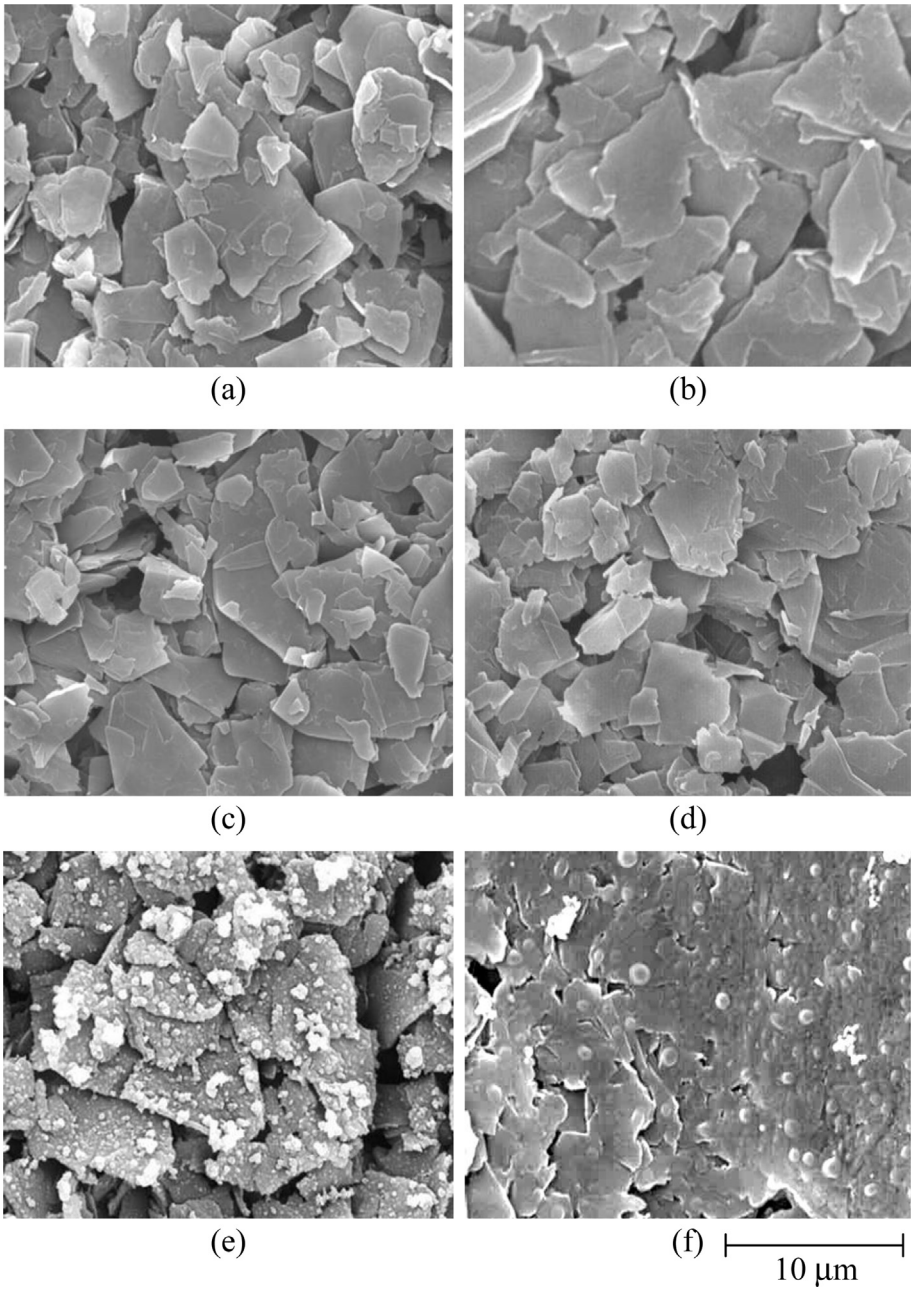

Fig. 4. FE-SEM images of NG-3 electrodes using PVdF and PAA as the binders (a, b) before soaking, (c, d) after soaking, and (e, f) after discharging up to 2.0 V *vs.* Li/Li^+ in the 1 mol dm^{-3} $LiClO_4$/EC + DEC (50:50 vol. %) electrolyte; (a, c, e) PVdF 10 wt. % and (b, d, f) PAA 10 wt. %.

a frequency response analyzer (NF Co., FRA5087). The impedance data were obtained in the frequency range of 100 kHz-10 mHz and with ac amplitude of ±10 mV.

The morphology observation and the surface analysis of the samples were carried out by scanning electron microscopy (JEOL, JSM-7001F, applied voltage 10 kV, working distance 10 mm, FE-SEM), energy dispersive X-ray spectroscopy (OXFORD, INCA X-act, applied voltage 10 kV, working distance 10 mm, EDX), and an X-ray photoelectron spectroscopy (Perkin Elmer, PHI 5600, XPS) analysis with Al Kα radiation ($h = 1486$ eV). Depth profiling was done by Ar ion-beam sputtering (3 kV), and the measured surface area was 16 mm^2 (4 mm × 4 mm). The specific surface areas of the samples were measured by the Brunauer–Emmett–Teller (B.E.T.) method using nitrogen adsorption (BEL SORP MINI, BEL JAPAN, Inc.) under liquid nitrogen (77 K) as the cooling medium. Before the measurement of the specific surface area, the suspension, which was prepared under the same conditions as those for the previously described electrode was evaporated to dryness, then dried at room-temperature for 24 h under reduced pressure. The samples were then dried in nitrogen at 120 °C for 3 h in the pre-treatment station (BEL PREP-flow, BEL JAPAN, Inc.). For the *ex situ* measurements of the graphite electrodes, the electrodes were charged at a constant current density of 175 mA g^{-1} to the specified potentials for 12 h. The cells were disassembled in the glove box to obtain the electrode samples. The obtained samples were then washed with DEC (Wako Pure Chemical Industries, Ltd., superfine quality). Prior to their use, the samples were dried at 25 °C for 12 h under reduced pressure.

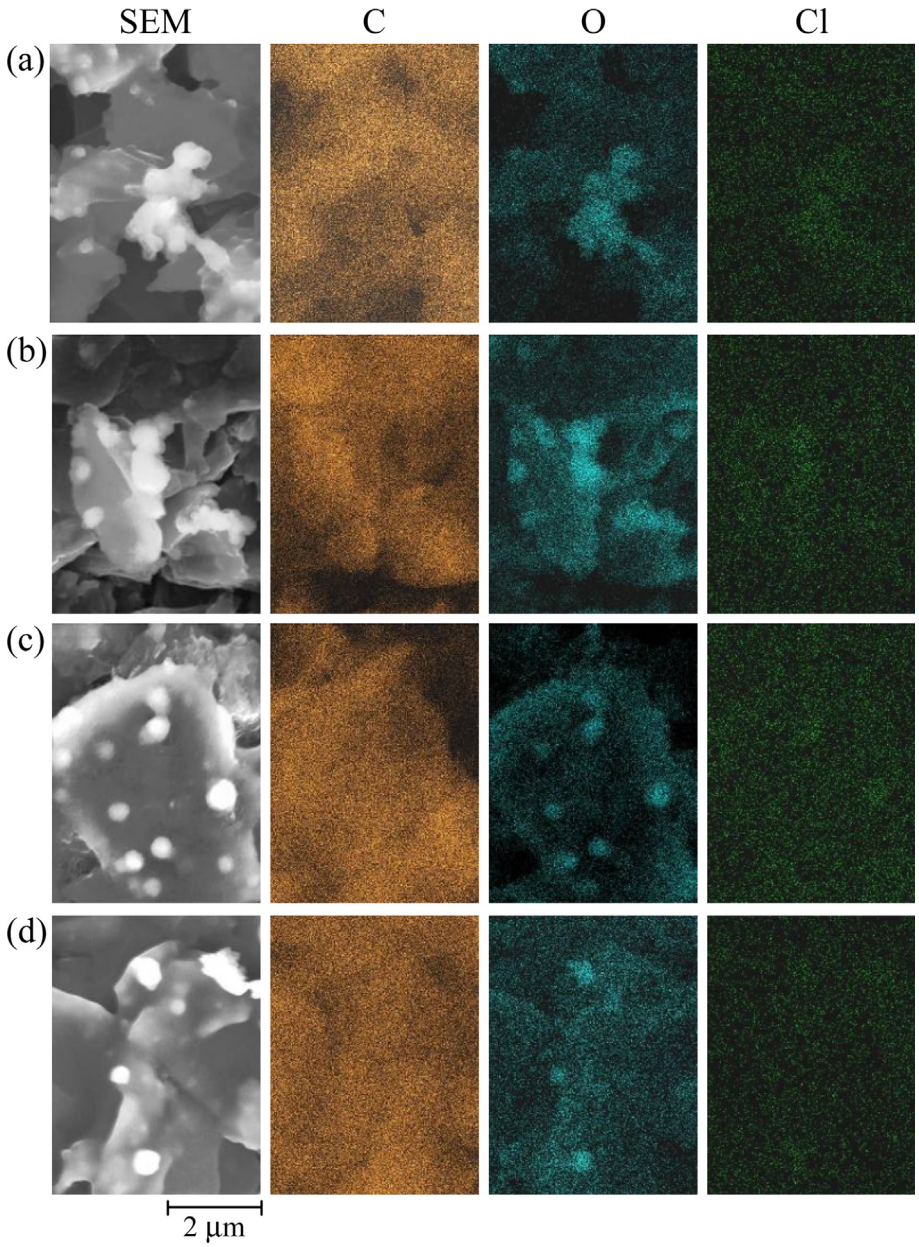

Fig. 5. FE-SEM images of NG-3 electrodes using PVdF and PAA as the binders after charging down to the prescribed potentials (*vs.* Li/Li^+) in the 1 mol dm^{-3} $LiClO_4$/EC + DEC (50:50 vol. %) electrolyte and corresponding EDX mappings for the C, O, and Cl elements; (a) PVdF 10 wt. % at 0.8 V, (b) PVdF 10 wt. % at 5 mV, (c) PAA 10 wt. % at 0.8 V, and (d) PAA 10 wt. % at 5 mV.

Table 1
Atomic concentrations at the surface of the NG-3 electrodes using PVdF and PAA as the binders before charging and after charging down to the prescribed potentials (*vs.* Li/Li^+) in the 1 mol dm^{-3} $LiClO_4$/EC + DEC (50:50 vol. %) electrolyte determined by EDX spectroscopy.

Binder	PVdF			PAA		
Element	C	O	Cl	C	O	Cl
Before charging	99.22	0.78	–	98.82	1.18	–
Charged down to 0.8 V	81.87	17.45	0.68	86.10	13.64	0.26
Charged down to 5 mV	74.35	25.35	0.30	65.11	34.66	0.22

(Unit: at.%).

3. Results and discussion

We have investigated the influence of the binder types on the initial charge–discharge characteristics. Fig. 1 shows the 1st charge–discharge curves of the NG-3 electrodes using (a) PVdF (10 wt. %) and (b) PAA (10 wt. %) as the binders [5]. In this paper, the cathodic polarization due to the Li^+ ion intercalation into the graphite layer is defined as a charge; the anodic polarization due to the Li^+ ion deintercalation is defined as a discharge. The 1st charge–discharge curves of the NG-3 electrode using PVdF as the binder (PVdF binder NG-3 electrode) showed that the discharge capacity and the charge–discharge efficiency at the 1st cycle were 342.8 mAh g^{-1} and 76.4%, respectively. In contrast, the 1st charge–discharge curves of the NG-3 electrode coated with PAA as the binder (PAA binder NG-3 electrode) showed that the discharge

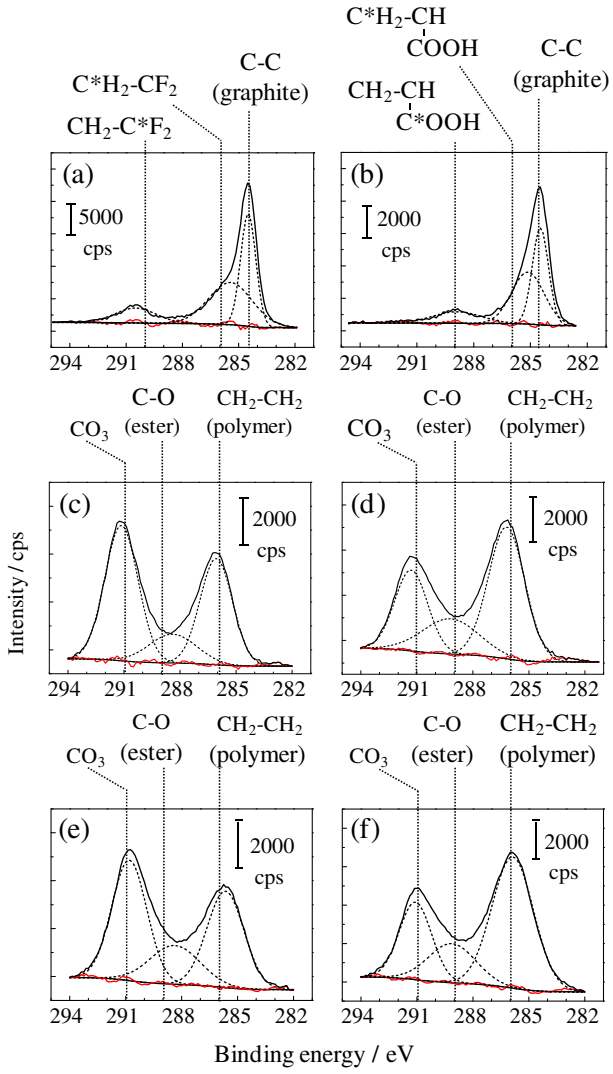

Fig. 6. High resolution XPS spectra (solid line) and their fitting curves (dashed line) of the C 1s region for the NG-3 electrodes using (a, c, e) PVdF and (b, d, f) PAA as the binders (a, b) before charging, (c, d) after charging down to 0.8 V, and (e, f) after discharging up to 2.0 V in the 1 mol dm^{-3} $LiClO_4$/EC + DEC (50:50 vol. %) electrolyte; solid line: etching time 0 min.

capacity and the charge–discharge efficiency were 356.7 mAh g^{-1} and 84.6%, respectively. As shown in Fig. 1, the difference between the PAA binder NG-3 electrode and the PVdF binder NG-3 electrode was very similar around 0.8 V, which was the potential at which lithium alkyl dicarbonate ($ROCO_2Li$) formed [10,11]. The main difference was observed below 0.2 V, which was the potential at which the SEI layer was almost formed. This suggested that the binder types might have an influence on the charge reaction.

In order to investigate the influence of the binder types on the coating, the B.E.T. specific surface area of the NG-3 particles using PAA and PVdF were measured (Fig. 2). For the PAA binder, the specific surface area gradually decreased along with the increased mixing ratio of PAA. The specific surface area employing the PAA binder (5 wt. %) was almost equal to that using the PVdF binder (10 wt. %). Therefore, this suggested that the surface of the NG-3 particles was effectively coated by employing PAA rather than PVdF.

The relationship between the B.E.T. specific surface area of the graphite particles and the irreversible capacity of the graphite electrode resulting from the formation of the SEI film on the 1st charge was examined (Fig. 3). In this study, the capacity, which subtracted the 1st discharge capacity from the 1st charge capacity,

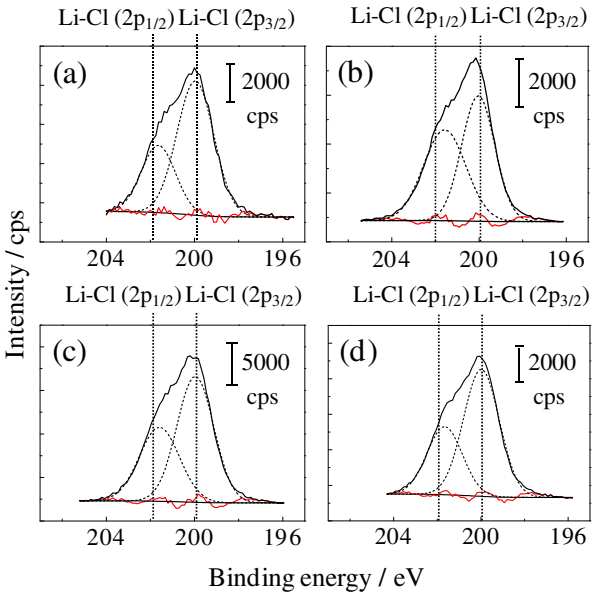

Fig. 7. High resolution XPS spectra (solid line) and their fitting curves (dashed line) of the Cl 2p region for the NG-3 electrodes using PVdF and PAA as the binders before charging and after discharging up to 2.0 V in the 1 mol dm^{-3} $LiClO_4$/EC + DEC (50:50 vol. %) electrolyte; solid line: etching time of 0 min; (a) PVdF 10 wt. % after charging down to 0.8 V (b) PAA 10 wt. % after charging down to 0.8 V (c) PVdF 10 wt. % after discharging up to 2.0 V, and (d) PAA 10 wt. % after discharging up to 2.0 V.

is defined as the irreversible capacity. The 1st discharge capacity, the 1st charge–discharge efficiency, and the irreversible capacity were 367.7 mAh g^{-1}, 67.7 mAh g^{-1}, and 84.5% for PAA 5 wt. %, 368.8 mAh g^{-1}, 66.8 mAh g^{-1}, and 84.7% for PAA 8 wt. %, 325.0 mAh g^{-1}, 51.5 mAh g^{-1}, and 86.3% for PAA 12.5 wt. %, respectively. As shown in Fig. 3, the irreversible capacity increased

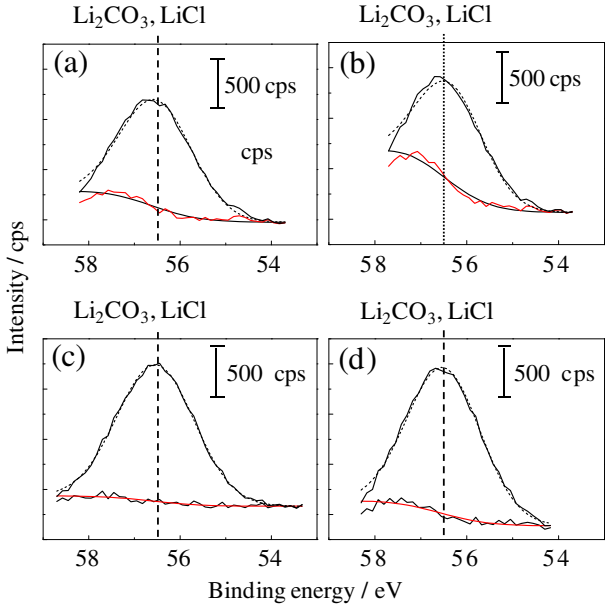

Fig. 8. High resolution XPS spectra (solid line) and their fitting curves (dashed line) of the Li1s region for the NG-3 electrodes using PVdF and PAA as the binders before charging and after discharging up to 2.0 V in the 1 mol dm^{-3} $LiClO_4$/EC + DEC (50:50 vol. %) electrolyte; solid line: etching time of 0 min; (a) PVdF 10 wt. % after charging down to 0.8 V, (b) PAA 10 wt. % after charging down to 0.8 V (c) PVdF 10 wt. % after discharging up to 2.0 V, (d) PAA 10 wt. % after discharging up to 2.0 V.

Table 2
Summary of XPS peak assignments shown in Figs. 6, 7, and 8.

Region	PVdF 10 wt.%			PAA 10 wt.%			Assignment	Ref.
	Before charge	Charge 0.8 V	Discharge 2.0 V	Before charge	Charge 0.8 V	Discharge 2.0 V		
C 1s (eV)	284.5			284.5			C–C (graphite)	[18–22]
				285.2			C^*H_2–CH(COOH)	[6,18,20,23]
	285.5						C^*H_2–CF_2 (polymer)	[20,22]
		286.1	285.7		286.2	285.9	CH_2–CH_2 (polymer)	[21]
				288.9			CH_2–CH(C^*OOH)	[6,20,22,23]
		288.5	288.4		289.2	289.1	C–O (ester)	[18,19,22]
	291.0						CH_2–C^*F_2	[6,20,22]
		291.1	290.8		291.3	291.1	CO_3	[18,21]
Cl 2p (eV)		199.9	199.9		200.0	199.9	LiCl ($2p_{3/2}$)	[18,20,22]
		201.7	201.6		201.6	201.7	LiCl ($2p_{1/2}$)	[18,20,22]
Li 1s (eV)		56.5	56.5		56.5	56.5	Li_2CO_3, LiCl	[18]

Note: Experimental values are shown in Table 2.

as the specific surface area of the graphite became greater. Especially, the irreversible capacity of the PVdF binder NG-3 electrode was very high compared to that of the PAA binder NG-3 electrode. Because the relationship between the B.E.T. surface area of the graphite particles and the irreversible capacity loss is well known [12], it was judged that this result agreed with the previous result. In addition, it was reported that the SEI formation occurred on the edge surface of the graphite [13–16]. Because the specific surface area of the graphite particles increased as the ratio of the edge surface increased [17], it was considered that the SEI formation reaction increased as the specific surface area increased. Based on these results, it was considered that the reductive decomposition of the electrolyte would be repressed on the 1st charge because the edge surface would be effectively coated with the PAA binder compared to the PVdF binder.

Fig. 4 shows the FE-SEM images of the PVdF binder NG-3 electrodes and the PAA binder NG-3 electrodes (a, b) before soaking, (c, d) after soaking, and (e, f) after 1st discharging up to 2.0 V. The NG-3 particles consisting of the average particle size of 3 μm and a scale-like particle shape were observed regardless of the binder types before soaking (a, b). The surface morphology of the particles did not change after soaking (c, d). The surface deposits were

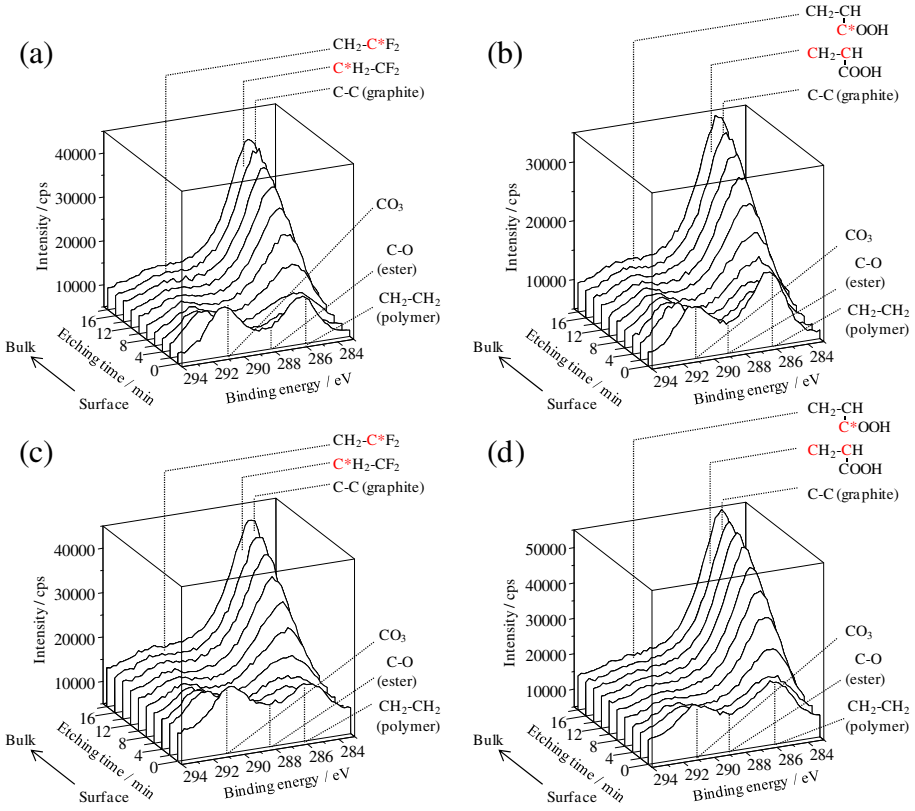

Fig. 9. High resolution XPS spectra of the C1s region measured after each etching of the NG-3 electrodes using PVdF and PAA as the binders after charging down to 0.8 V and after discharging up to 2.0 V in the 1 mol dm^{-3} $LiClO_4$/EC + DEC (50:50 vol. %) electrolyte; etching time: every 2 min from 0 to 18 min; (a) PVdF 10 wt. % after charging down to 0.8 V, (b) PAA 10 wt. % after charging down to 0.8 V, (c) PVdF 10 wt. % after discharging up to 2.0 V, and (d) PAA 10 wt. % after discharging up to 2.0 V.

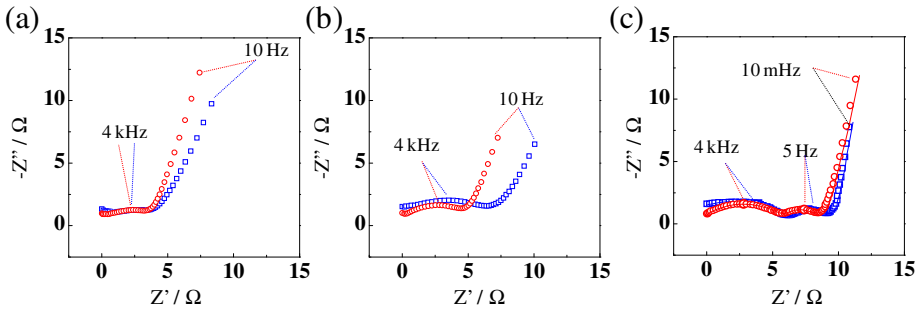

Fig. 10. Nyquist plots for the NG-3 electrodes using PVdF and PAA as the binders charged down to the prescribed potentials (*vs.* Li/Li^+) in the 1 mol dm^{-3} $LiClO_4$/EC + DEC (50:50 vol. %) electrolyte; Frequency range: 100 kHz–10 mHz, AC amplitude: ±10 mV; (a) 1.0 V, (b) 0.8 V, (c) 0.2 V; (○) PAA 10 wt. %; (□) PVdF 10 wt. %.

observed on the surface of the NG-3 particles after 1st discharging up to 2.0 V (e, f). Mori et al. reported that the surface deposits were the products due to the reductive decomposition of the electrolyte [14], suggesting that the surface deposits would be a part of the SEI.

Fig. 5 shows the FE-SEM images and corresponding EDX mappings of the NG-3 electrodes using (a, b) PVdF (10 wt. %) and (c, d) PAA (10 wt. %) as the binders after charging down to (a, c) 0.8 V and (b, d) 5 mV. Reductive decomposition of the electrolyte occurred on the surface of the NG-3 particles regardless of the binder types after charging down to 0.8 V. In addition, a greater amount of the surface deposit was observed on the surface of the PVdF binder NG-3 electrode. The EDX mapping results showed that C, O, and Cl were detected on the surface of both electrodes. Cl existed on the entire surface of the particle, whereas O locally existed as a surface deposit. Regarding fluorine, even if the binder was PVdF, the fluoride concentration on the surface of the PVdF binder NG-3 electrode was under the detection limit. The results indicated that these elements (O and Cl) were the same as those of a conventional SEI. Based on the above SEI formation mechanism, the inorganic component was mainly formed at a potential nobler than 0.8 V [10,11]. Large amounts of O and Cl are contained in the inorganic component that has been reported to be Li_2CO_3 or LiCl. The EDX mappings showed that the distribution of the surface deposit at 0.8 V almost corresponded to that of O and Cl, suggesting that the surface deposit would be the inorganic component. White deposits are thought to be a high-resistance area in the FE-SEM images because they were caused by charging.

The atomic concentrations at the surface of the NG-3 electrodes using PVdF (10 wt. %) and PAA (10 wt. %) as the binders at each potential for the 1st charging process determined by EDX spectroscopy are summarized in Table 1. The percentage of O in the PAA binder NG-3 electrode was higher than that in the PVdF binder NG-3 electrode before charging, indicating that this would be due to the differences in the amount of O in the binder. The decrease in C, the increase in O, and the generation of Cl were detected regardless of the binder types after charging down to 0.8 V, suggesting that Li_2CO_3 and LiCl would be formed as reported in the literature [10,11]. In contrast, the PAA binder NG-3 electrode showed a low percentage of O and Cl, suggesting that the formation of these inorganic compounds would be repressed. C and Cl decreased and O increased regardless of the binder types after charging down to 5 mV, suggesting that $ROCO_2Li$ would be formed.

The chemical composition of the surface deposit was investigated by XPS and then the difference between the PAA binder and the PVdF binder was discussed. Fig. 6 shows the high-resolution XPS spectra of the C 1s region for the NG-3 electrodes using (a, c, e) PVdF (10 wt. %) and (b, d, f) PAA (10 wt. %) as the binders (a, b) before charging, (c, d) after charging down to 0.8 V, and (e, f) after discharging up to 2.0 V. The peaks were detected at around 284.5 eV and 286.0 eV on the surface of both electrodes before charging (Fig. 6(a) and (b)). The sharp peak at around 284.5 eV was assigned to graphite (C–C) [18–22]. The peak at around 286.0 eV was assigned to hydrocarbons, i.e., $-CH_2-CH_2-$ type bonds in the polymers. Thus, C* did not locate next to F in the PVdF binder NG-3 electrode [20,22], whereas C* did not locate next to O in the PAA binder NG-3 electrode [6,18,20,23]. The peak at around 290.0 eV was assigned to C* located next to F in the PVdF binder NG-3 electrode [6,20,22] and the carboxyl carbon on the PAA binder NG-3 electrode [6,20,22,23]. In addition, the peaks of NG-3 and both binders existed on the surface of the NG-3 electrode before charging. The strong peak of the graphite (C–C) thus was detected regardless of the binder types before charging, suggesting that the surface of the NG-3 particles was not completely covered.

The peaks were detected at around 286.0 eV and 291.0 eV on the surface of the NG-3 electrodes regardless of the binder types after charging down to 0.8 V (Fig. 6(c) and (d)) and discharging up to 2.0 V (Fig. 6(e) and (f)). Although the peak at around 286.0 eV was assigned to hydrocarbons in the polymers [21], the peak positions shifted slightly higher than the above peak position of the binder. According to a report about the SEI analysis by XPS [19], this peak

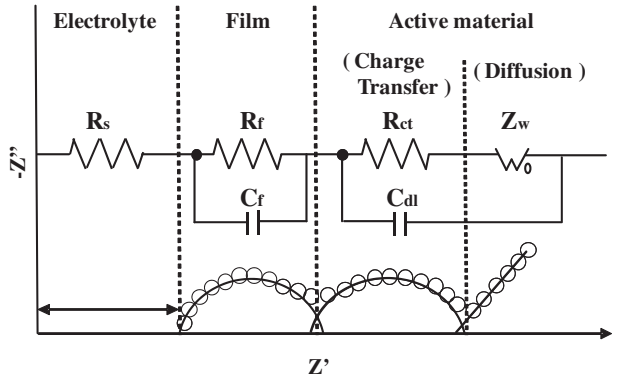

Fig. 11. Equivalent circuit used for the analysis of the impedance plots shown in Fig. 8(c); R_s: solution resistance, C_f and R_f: capacitance and resistance, respectively, of the surface film; C_{dl}: electrical double-layer capacitance; R_{ct}: charge transfer resistance; Z_W: Warburg impedance [24].

Table 3
The parameters for the NG-3 electrodes shown in Fig. 10(c) obtained by fitting with the equivalent circuit shown in Fig. 11.

Binder	R_{sol} [Ω cm^2]	R_f [Ω cm^2]	C_f [μF cm^{-2}]	R_{ct} [Ω cm^2]	C_{dl} [mF cm^{-2}]	Z_w [Ω cm $s^{-1/2}$]
PVdF	27.23	9.82	609	1.82	15.99	5.45
PAA	36.69	7.34	781	1.56	9.83	3.78

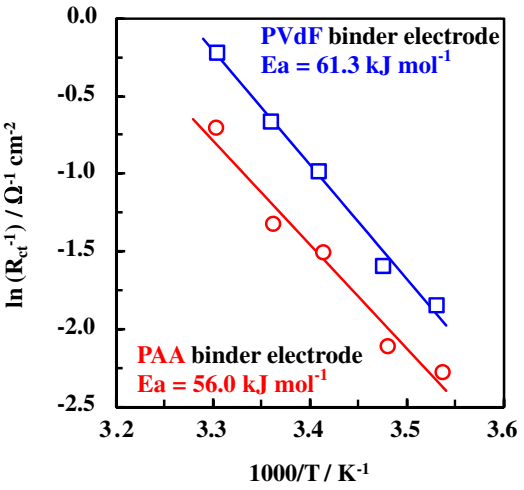

Fig. 12. Temperature dependence of charge-transfer resistances at a potential of 0.2 V. The activation energies were obtained from the slope.

was assigned to a hydrocarbon in polyethylene oxide (PEO). The peak at around 291.0 eV was assigned to a carbonate [18,21]. These peak positions were close to the position of C located next to F in the PVdF binder NG-3 electrode before charging. However, the results of the EDX mappings shown in Fig. 5 showed that the fluoride concentration in the surface of the PVdF binder NG-3 electrode was under the detection limit after charging down to 0.8 V and 5 mV, suggesting that these peaks were assigned to the carbonate (Fig. 6(c) and (e)). The results showed that not only the formation of an inorganic component, but also that of an organic component started at 0.8 V. The peak at around 289.2 eV was assigned to an ester carbon in the PAA binder NG-3 electrode [18,19,22]. It should be noted that the ratios of the hydrocarbon and carbonate in the SEI composition were different based on the binders. Thus, the ratio of carbonate was low in the PAA binder NG-3 electrode. Considering the SEI mechanism using the results of the EDX mappings, this carbonate was mainly assigned to Li_2CO_3 at 0.8 V, suggesting that the SEI layer with a small ratio of an inorganic component was formed in the PAA binder NG-3 electrode.

Fig. 6(e) and (f) shows that the spectra after discharging up to 2.0 V were almost the same as those after charging down to 0.8 V, suggesting that the formed SEI layer would be stable during the charge–discharge process after charging down to 0.8 V. Based on these results, it was found that the amount of the inorganic components of the SEI on the surface of the PAA binder NG-3 electrode was lower than that of the SEI on the surface of the PVdF binder NG-3 electrode.

Fig. 7 shows the high-resolution XPS spectra of the Cl 2p region for the NG-3 electrodes using (a, c) PVdF (10 wt. %) and (b, d) PAA (10 wt. %) as the binders (a, b) after charging down to 0.8 V and (c, d) after discharging up to 2.0 V, respectively. These peaks were assigned to the chlorine of a Li–Cl bond [18,20,22] because they were detected at around 200 eV on the surface of both electrodes.

Fig. 8 shows the high-resolution XPS spectra of the Li 1s region for the NG-3 electrodes using (a, c) PVdF (10 wt. %) and (b, d) PAA (10 wt. %) as the binders (a, b) after charging down to 0.8 V and (c, d) after discharging up to 2.0 V, respectively. These peaks were detected at around 56.5 eV on the surface of both electrodes after charging down to 0.8 V. These peaks could not be separated because they appeared at the same position. However, considering the results of the above-mentioned C 1s and Cl 2p, this peak would be assigned to a Li–O bond derived from Li_2CO_3 or a Li–Cl bond derived from LiCl.

According to Figs. 6–8, it was clarified that Li_2CO_3 and LiCl were formed on the surface of the NG-3 particles regardless of the binder types after charging down to 0.8 V. Based on these results, the XPS results of Figs. 6–8 are summarized in Table 2. These peak positions of each bond on the NG-3 electrodes were assigned to the bonds in Table 2.

In order to investigate the difference in the SEI composition in more detail, a depth profile analysis of the NG-3 electrode surface was carried out. Fig. 9 shows the high-resolution XPS spectra of the C 1s region measured after each etching of the NG-3 electrodes using (a, c) PVdF (10 wt. %) and (b, d) PAA (10 wt. %) as the binders (a, b) after charging down to 0.8 V and (c, d) after discharging up to 2.0 V, respectively. All spectra before etching were the same as those shown in Fig. 6(c, d, e, f).

In both electrodes, the shape of the spectra changed with the etching and then peaks appeared at around 284.5 eV (graphite (C–C)). It was found that the surface of the electrode was covered with a surface deposit at 0.8 V regardless of the binder types because these peaks of the SEI disappeared during etching and then the peak of graphite appeared. The peak intensity of the carbonate derived from Li_2CO_3 in the inorganic components was the strongest at the outermost surface and decreased during the etching. The peak intensity of the carbonate derived from Li_2CO_3 in the inorganic components on the surface of the PAA binder NG-3 electrode was weaker than that of the PVdF binder NG-3 electrode. Based on these results, it was found that the formation of the inorganic components of the SEI on the surface of the PAA binder NG-3 electrode would be suppressed compared to those on the PVdF binder NG-3 electrode.

Fig. 10 shows the Nyquist plots for the NG-3 electrodes coated with PVdF (10 wt. %) and PAA (10 wt. %) as the binders after charging down to (a) 1.0 V, (b) 0.8 V, and (c) 0.2 V. The arcs attributed to the surface deposits, which were the formed passive film, were observed at 1.0 V. The arcs attributed to the passive film were expanded at 0.8 V compared to 1.0 V. Moreover, two arcs

Table 4
The activation energies at the interface between the NG-3 electrode and the 1 mol dm^{-3} $LiClO_4$/EC + DEC (50:50 vol. %) electrolyte at a potential of 0.2 V shown in Fig. 12.

Electrode	Activation energy (kJ mol^{-1})	Ref.
PAA binder NG-3 electrode	56.0	This study
PVdF binder NG-3 electrode	61.3	This study
HOPG	50–60	[25]
HIP-treated carbon	61.5 ± 2.0[a]	[26]

[a] Measured at a potential of 0.8 V.

Table 5
Summary of the advantages of the NG-3 electrode coated with the PAA binder at each potential during first charging.

Potential	Advantage of the PAA binder	Methods
Before charging	Edge surface was effectively covered.	B.E.T.
1.0 V	Resistance of the NG-3 electrode was lower.	EIS
0.8 V	Fewer inorganic deposits on the electrode.	SEM/EDX
	The ratio of the inorganic components was lower.	XPS
0.2 V	Film resistance of the NG-3 electrode was lower.	EIS
After discharging	The first charge–discharge efficiency was higher.	Charge–discharge test
	Fewer inorganic deposits on the electrode.	SEM/EDX
	The ratio of the inorganic components was lower.	XPS

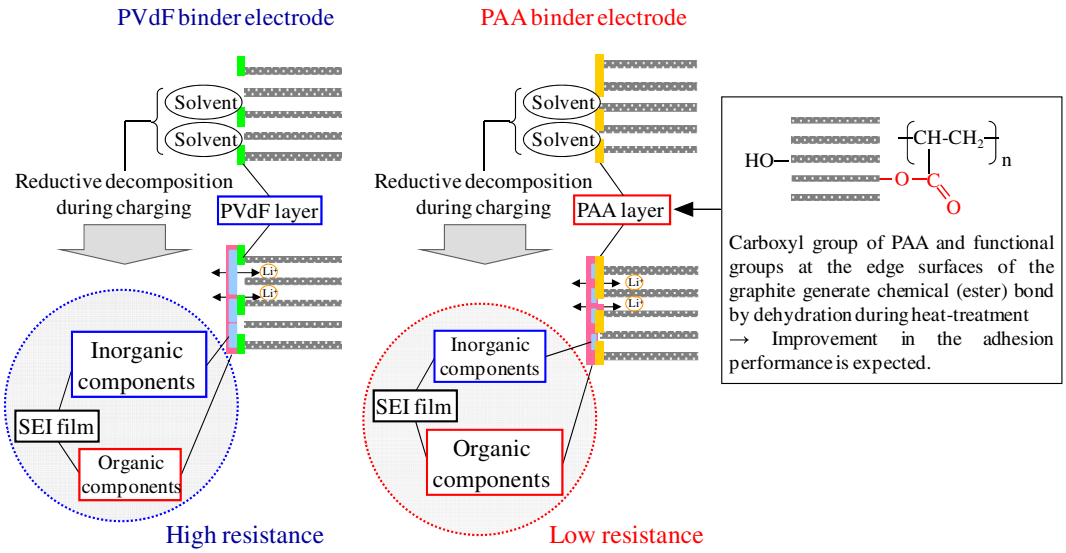

Fig. 13. A schematic model describing the influence of the binder types on the SEI formation reaction and surface deposit of the NG-3 electrode.

clearly appeared at 0.2 V. The resistance attributed to the SEI film formation increased during charging because the SEI film resistance at 0.2 V increased compared to the SEI film resistance at 0.8 V. It was considered that the arc in the low-frequency area was ascribed to the charge transfer resistance in the interface between the SEI film and the electrode. The resistance of the PAA binder NG-3 electrode was lower than that of the PVdF binder NG-3 electrode at each potential. It was considered that the SEI film formed during charging would have an influence on the interface resistance. It was considered that the inorganic component in the SEI was the cause of the increased passive film resistance because the ionic conductive layer of Li^+ ions in the SEI was the organic component such as PEO. Based on these results of the charge–discharge cycle tests, it was considered that the reductive decomposition of the electrolyte would be repressed at higher than 0.8 V. In addition, based on these results of the above-mentioned surface analysis, the percentage of the inorganic components of the SEI on the surface of the PAA binder NG-3 electrode was low. Therefore, it was considered that the difference in the SEI film component would have an influence on the SEI film resistance.

Fig. 11 shows the equivalent circuit [24] employed for analysis of the Nyquist plots shown in Fig. 10(c). In this study, the Nyquist plots consisted of two arcs because the SEI film was formed on the surface of the NG-3 electrode. By considering two parallel RC circuits in series, one for the SEI film formation and the other for the intercalation of Li^+ ions, the equivalent circuit including two time constants was employed.

The parameters of the NG-3 electrodes shown in Fig. 10(c) obtained from the simulation for the equivalent circuit shown in Fig. 11 are summarized in Table 3. Concerning the SEI film component of the PAA binder NG-3 electrode, the film resistance R_f was low and the capacitance of the film C_f was high. As described above, it was considered that the difference in the formed passive film component would have an influence on the film resistance R_f. In this case, it is considered that the parallel circuit is located at the interface between the electrolyte and the SEI film because C_f is the capacitance of the SEI film. For the PAA binder NG-3 electrode, it was thus considered that the interfacial area between the electrolyte and the SEI film was larger because C_f was higher; the Li^+ ion in the SEI film would be easily transmitted because R_f was lower. On the other hand, regarding the parameters, the charge transfer resistance R_{ct}, the electrical double-layer capacitance C_{dl}, and the Warburg impedance Z_w were low in the PAA binder NG-3 electrode, indicating that the charge transfer at the PAA binder NG-3 electrode easily occurred compared to that of the PVdF binder NG-3 electrode. The $R_{ct}C_{dl}$ parallel circuit is assumed in the electrochemical reaction field in general. The $R_{ct}C_{dl}$ parallel circuit is located at the interface between the electrolyte and the film in the case of the electronic conductivity or at the interface between the film and the electrode in the case of the ionic conductivity. In this study, the $R_{ct}C_{dl}$ parallel circuit was located at the interface between the SEI film and the electrode because the formed SEI film had a Li^+ ion conductivity and clearly did not have any electronic conductivity. The C_{dl} of the PAA binder NG-3 electrode was low compared to that of the PVdF binder NG-3 electrode, indicating a low surface area. This result agrees with the measured results of the B.E.T. specific surface area shown in Figs. 2 and 3. The Z_w that appears in the low-frequency area represents the impedance due to the diffusion of the Li^+ ions inside the electrode. It was considered that the Li^+ ion in the PAA binder NG-3 electrode would be easily diffused compared to the PVdF binder NG-3 electrode because the Z_w of the PAA binder NG-3 electrode was lower.

Furthermore, the temperature dependence of the charge-transfer resistances for the NG-3 electrodes at 0.2 V obtained from the Nyquist plots in Fig. 10(c) is shown in Fig. 12. The activation energies were obtained from the slope. The charge transfer resistances decreased with increasing temperature and showed an Arrhenius-type behavior. The activation energies of the charge-transfer resistances were 56.0 kJ mol^{-1} for the PAA binder NG-3 electrode and 61.3 kJ mol^{-1} for the PVdF binder NG-3 electrode. As summarized in Table 4, these values were almost equal to that obtained for the lithium-ion transfer at an HOPG and a HIP-treated carbon electrodes [25,26]. Based on these results, it was clarified that the Li^+ ion in the PAA binder NG-3 electrode was more easily conducted compared to the Li^+ ion in the PVdF binder NG-3 electrode.

Based on these results and the knowledge obtained in this study, the advantages of the PAA binder NG-3 electrode at each potential for the 1st charging process are summarized in Table 5. The B.E.T. specific surface area measurement results indicated that the edge surface was effectively coated before charging. The film resistance was low at 1.0 V as indicated by the AC impedance. The FE-SEM/EDX observations showed that a small amount of a surface deposit of inorganic components derived from Li_2CO_3

or LiCl was observed on the surface of the electrode at 0.8 V. The XPS results showed that the percentage of the inorganic components in the film was relatively low. The AC impedance results showed that the SEI film resistance was low at 0.2 V. The charge–discharge cycle tests results showed that the 1st charge–discharge efficiency was high after discharging up to 2.0 V. The FE-SEM/EDX observations indicated that a small amount of a surface deposit derived from the inorganic components was observed on the surface of the electrode. The XPS results represented that the percentage of the inorganic components of the film were relatively low. Based on these results, it was considered that the reductive decomposition of the electrolyte would be repressed on the 1st charge because the edge surface was effectively coated by the PAA binder, indicating that the SEI film had a low ratio of inorganic component formed on the PAA binder NG-3 electrode, although the components consisting of an organic component ($ROCO_2Li$) and an inorganic component (Li_2CO_3 and LiCl) in the SEI film were the same as those previously reported.

Fig. 13 illustrates a schematic model describing the influence of the binder types on the SEI formation reaction and surface deposit of the NG-3 electrode. Functional groups exist on the surface of the carbon materials [27]. Esterification between the edge of the graphite and the carboxyl group has taken place, and the PAA was strongly sorbed on the surface of the graphite [28–30]. NG-3 was effectively coated with PAA as a binder. The resistance of the electrode interface was low because the ratio of an organic component in the SEI film was high. Therefore, it can be reasonably concluded that the coating state of the binders had an influence on the SEI formation and the chemical composition.

4. Conclusion

We investigated the SEI formation reaction and surface deposit of a natural graphite (NG-3) electrode using the PAA binder and the conventional PVdF binder for comparison in an ethylene carbonate-based electrolyte, and obtained the following results.

1. The difference in the irreversible capacity of the 1st cycle was explained by the difference in the B.E.T. specific surface area, suggesting that the reductive decomposition of the electrolyte would be repressed on the 1st charge because the edge surface would be effectively coated with the PAA binder.
2. The SEI film with a low inorganic component ratio was formed in the case of the PAA binder NG-3 electrode.
3. It was clarified that the Li^+ ion in the PAA binder NG-3 electrode was easily conducted compared to the Li^+ ion in the PVdF binder NG-3 electrode.

Therefore, it was concluded that the coating state of the binders had an influence on the initial charge–discharge characteristics, the SEI formation reaction, and the SEI film composition.

Acknowledgments

This work was partially supported by a Grant-in-Aid for Scientific Research from the Japanese Ministry of Education, Science, Sports and Culture (No. 21550169).

References

[1] M. Gaberscek, M. Bele, J. Drofenik, R. Dominko, S. Pejovnik, Electrochem. Solid-State Lett. 3 (2000) 171.
[2] R. Dominko, M. Gaberscek, M. Bele, J. Drofenik, E.M. Skou, A. Würsig, P. Novák, J. Jamnik, J. Electrochem. Soc. 151 (2004) 1058.
[3] J. Drofenik, M. Gaberscek, R. Dominko, F.W. Poulsen, M. Mogensen, S. Pejovnik, J. Jamnik, Electrochim. Acta 48 (2003) 883.
[4] C.C. Li, J.T. Lee, X.W. Peng, J. Electrochem. Soc. 153 (2005) A809.
[5] K. Ui, S. Kikuchi, F. Mikami, Y. Kadoma, N. Kumagai, J. Power Sources 173 (2007) 518.
[6] S. Komaba, T. Ozeki, K. Okushi, J. Power Sources 189 (2009) 197.
[7] A. Magasinski, B. Zdyrko, I. Kovalenko, B. Hertzberg, R. Burtovyy, C.F. Huebner, T.F. Fuller, I. Luzinov, G. Yushin, Appl. Mater. Interfaces 2 (2010) 3004.
[8] Z. Zhang, T. Zeng, C. Qu, H. Lu, M. Jia, Y. Lai, J. Li, Electrochim. Acta 80 (2012) 440.
[9] K. Ui, J. Towada, S. Agatsuma, N. Kumagai, K. Yamamoto, H. Haruyama, K. Takeuchi, N. Koura, J. Power Sources 196 (2011) 3900.
[10] A. Naji, J. Ghanbaja, B. Humbert, P. Willmann, D. Billaud, J. Power Sources. 63 (1996) 33.
[11] G.-C. Chung, H.-J. Kim, S.-I. Yu, S.-H. Jun, J.-w. Choi, M.-H. Kim, J. Electrochem. Soc. 147 (2000) 4391.
[12] K. Zaghib, G. Nadeau, K. Kinoshita, J. Electrochem. Soc. 147 (2000) 2110.
[13] M. Inaba, Z. Siroma, A. Funabiki, Z. Ogumi, T. Abe, Y. Mizutani, M. Asano, Langmuir. 12 (1996) 1535.
[14] S. Mori, H. Asahina, H. Suzuki, A. Yonei, K. Yokoto, J. Power Sources. 68 (1997) 59.
[15] K.A. Hirasawa, T. Sato, H. Asahina, S. Yamaguchi, S. Mori, J. Electrochem. Soc. 144 (1997) L81.
[16] A.C. Chu, J.Y. Josefowicz, G.C. Farrington, J. Electrochem. Soc. 144 (1997) 4161.
[17] M. Winter, P. Novák, A. Monnier, J. Electrochem. Soc. 145 (1998) 428.
[18] D. Aurbach, B. Markovsky, A. Shechter, Y. Ein-Eli, J. Electrochem. Soc. 143 (1996) 3809.
[19] A.M. Andersson, K. Edström, J. Electrochem. Soc. 148 (2001) A1100.
[20] J. Arai, H. Katayama, H. Akahoshi, J. Electrochem. Soc. 149 (2002) A217.
[21] H. Ota, Y. Sakata, A. Inoue, S. Yamaguchi, J. Electrochem. Soc. 151 (2004) A1659.
[22] J. Chastain, J.F. Moulder, W.F. Stickle, P.E. Sobol, K.D. Bomben, Handbook of X-ray Photoelectron Spectroscopy, Perkin-Elmer Co., 1992, p. 216.
[23] S. Komaba, K. Shimomura, N. Yabuuchi, T. Ozeki, Hi Yui, K. Konno, J. Phys. Chem. C. 115 (2011) 13487.
[24] T. Piao, S.-M. Park, C.-H. Doh, S.-I. Moon, J. Electrochem. Soc. 146 (1999) 2794.
[25] T. Abe, H. Fukuda, Y. Iriyama, Z. Ogumi, J. Electrochem. Soc. 151 (2004) A1120.
[26] T. Doi, K. Miyatake, Y. Iriyama, T. Abe, Z. Ogumi, T. Nishizawa, Carbon 42 (2004) 3183.
[27] J.L. Figueiredo, M.F.R. Pereira, M.M.A. Freitas, J.J.M. Órfao, Carbon 37 (1999) 1379.
[28] T. Osa, U. Akiba, I. Segawa, J.M. Bobbitt, Chem. Lett. 17 (1988) 1423.
[29] T. Osa, Electrochemistry 69 (2001) 560.
[30] N. Ding, J. Xu, Y. Yao, G. Wegner, I. Lieberwirth, C. Chen, J. Power Sources 192 (2009) 644.